to be published in J. Vac Sci. Technol B Nov/Dec 2000

Evaluation of a 100 kV TFE Electron Beam Nanolithography System

D.M. Tennant and R. Fullowan[1]
Bell Laboratories/ Lucent Technologies
Holmdel, NJ 07733
[1]Murray Hill, NJ 07728

H. Takemura, M. Isobe, and Y. Nakagawa
JEOL Ltd
Akishima Tokyo 196-8558 JAPAN

ABSTRACT

We report on the results of a series of performance evaluation tests of a JEOL model JBX-9300FS electron beam nanolithography system -a next generation spot beam lithography tool. The electron optics feature a high brightness thermal field emission cathode, 100 kV accelerating voltage, and a two stage deflector which is currently operating at a 25MHz deflection rate. The system is the first to use a high precision 20 bit DAC to achieve 1 nm addressability over a 500 μm writing field. The stage has a 255 x 235 mm range of motion in X and Y, respectively and is configured to load 300mm wafers. The stage is positioned with a laser interferometer with a resolution of 0.6 nm.

The system was tested for criteria which will be needed to excel in the areas of lithographic resolution, stability, exposure uniformity and pattern placement accuracy. A minimum spot size of 4 nm was measured at a current of 100 pA. The spot remained below 6.5 nm for beam currents up to 8 nA. Maximum DAC linearity errors were found to be below 0.5 LSB which corresponds to 0.5 nm. Pattern placement accuracy in a 50 mm square area was found to be within +/- 16 nm and inside the 500 μm writing field within +/- 7 nm. The good uniformity was obtained for exposures of 50 nm period gratings over all regions of 400 μm square area. This indicates that the dynamic focus and stigmation method which has been implemented is viable for nanolithography over large fields.

I. INTRODUCTION

While high voltage e-beam lithography has been known for many years in the research community as having advantages for ultra high resolution lithography [1-5], only recently have a small number of vendors offered 100 kV combined with a full commercial system [6,7]. The JBX-9300FS is the first 100 kV spot beam electron beam exposure system developed by JEOL and represent the most recent commercial offering. The electron optics feature a high brightness thermal field emission cathode, 100 kV accelerating voltage, and a two stage deflector which is currently operating at a 25MHz deflection rate. The system is the first to use a high precision 20 bit DAC to achieve 1 nm addressability over a 500μm writing field. The high scanning rate is achieved via a 12-bit sub-field deflector. The stage has a 255 x 235 mm range of motion in X and Y.

respectively. The stage is configured to load cassettes large enough to accommodate 300mm wafers or 230 mm (9 inch) mask blanks. The stage is positioned with a Agilent laser interferometer with a resolution of 0.6 nm. The system shares a common platform and data stream with JEOL's shaped-beam system, the JBX-9000MV, which is intended for commercial mask production. The system being installed at Bell Laboratories/ Lucent Technologies is the second such system built by JEOL. The first was delivered to NEC in 1998 and the performance at 50 kV was previously reported [8]. This is the first report to our knowledge of this system at the design condition of 100 kV.

II. PERFORMANCE TEST RESULTS

The system was tested at the JEOL factory in the major performance areas prior to disassembly for shipment to Bell Labs. All tests were completed at an operating voltage of 100 kV. Many of the results discussed individually here are summarized in Table 1.

IIa. Column Performance

The diameter of the focused electron beam can be a limiting factor in nanolithography and therefore is an important performance criterion. The minimum spot size was measured using a knife edge test in which the signal trace obtained from a transmission detector located below a knife edge sample is displayed on a digital storage scope as the beam is scanned over an edge. The vendor specification and the measurement represent the width corresponding to the 15% to 85% signal points in the rise time. Since the minimum useable beam current is judged to be 50 pA, a value slightly higher, 100 pA, was used to evaluate the minimum spot. Scope traces were obtained for the transmitted signal for scans in X and Y. Using the laser interferometer controlled stage to calibrate the scan, beam widths along both axes are found to be about 4 nm. Similar measurements were made for various higher beam currents adjusted upward to 8 nA. As the plot in Fig. 1 shows, the beam diameter remained below 6 nm for all currents throughout the measurement range. The lines plotted on the graph are the calculated aberration-limited performance for various aperture sizes. Reasonably good agreement is observed for the smallest aperture (60 μm dia) while smaller than expected spot sizes were measured for the 100 μm aperture.

Since there are circumstances under which the spot can be too small for the stepping distance, larger apertures have been included (but not yet measured). The upper dashed lines in Fig. 1 show the expected beam size for the 200 μm and 300 μm diameter apertures. These aperture choices are a means of obtaining the larger spot sizes needed to extend the useable range of currents. The beam current limit under normal use will likely be about 30 nA, however, the calculations show that 100 nA may be possible. Figure 2 plots the calculated current densities for the measured spot sizes. The smallest aperture produced current densities in the range 800 to 15,000 A/ cm^2 . This increases to over 30,000 A/cm^2 for the 100 μm aperture.

Previous generations of JEOL EBL systems featured a two objective lens system, one with high resolution but a small scanning field and a second with moderate resolution but a large scanning field. The JBX-9300FS achieves both goals in a single lens design. This requires, however, implementation of dynamic focus and stigmation in order to maintain linewidth control within the large writing field due to the larger deflection angle (+/- 5 mR). One of the current user applications particularly dependent on the quality of

these adjustments is the high electron mobility transistor (HEMT) work. Typical designs include wide gate transistors which make use of full field width 0.1 μm gate lengths. In order assure that the new system meets the required focus uniformity, we exposed 0.1μm (nominal) crosses at the center, edges and corners of a maximum writing field (500 μm). SEM images of all nine locations are shown in Fig. 3. Linewidths were measured at each location using a CD measurement SEM. The results showed that the mean of the X widths was 103 nm with maximum deviations in the range +/- 3% and that of the Y values were 107 nm +/- 3%, both well within the conservative factory spec of +/- 15%.

To more critically test the dynamic focus and stigmation function for use in nanolithography applications (e.g., micro-Fresnel zone plates), finer patterns were exposed at the extrema of a slightly smaller (400 μm) writing field using the dynamic correction function. Fig 4. shows the resultant exposures made of a 50 nm period (25 nm line and space) pattern at various locations within the writing field. The good uniformity for both X and Y in these exposures indicates that the dynamic focus and stigmation method is viable for nanolithography applications over large fields. The same pattern was used to obtain a minimum linewidth. Figure 5 shows one result obtained in ZEP 520 resist, 18 nm lines on a 53 nm pitch.

Beam current stability is an important property for lithography instruments since both short term "flicker" as well as long term changes in the beam current can be important for exposure uniformity. The short term stability contributes to the linewidth control over short distances (e.g., duty cycle variations within a grating or gate length variations, etc.) while the long term stability determines the dose variations during exposure (e.g., systematic duty cycle or gate length changes across a workpiece). Short and long term variations in beam current were measured for two different condenser lens settings, corresponding to a low and a high beam current. The measurement was made at 100 pA and 2 nA for the short term and 100 pA and 2.5 nA for the long term test using a picoammeter connected to a Faraday cup. Both time tests indicated very small relative changes over the sampled periods for both current settings. The short term changes were nearly absent and only a small variation (0.4%) ocurred over the longer, fourteen hour test period.

Drift in the origin position of the beam is a common limitation for a variety of electron beam lithography applications. The most desirable mode of operation is to calibrate the instrument at the beginning of an exposure and rely on the inherent stability of the beam position in the electron optical column. This avoids the random measurements errors introduced during cyclic calibrations. This ideal situation is foiled when the beam drifts away from its initial position during the exposure, necessitating periodic registrations. The specification for beam drift in this instrument is 150 nm per hour. Figure 6 plots the measured drift for the JBX-9300FS over a 14 hour period. Measurements of the X and Y position change were made on two marks at different Z heights. The four drift plots indicate that the beam remained within 60 nm of its original position in X and within 25 nm in Y over the entire measurement period.

The 100 kV gun power supply was evaluated for stable output. This is also an important component since variations in accelerating voltage cause corresponding field size variations and hence stitching errors during exposure. To evaluate the high voltage stability, we measured the short and long term variations in the high voltage output. The high frequency ripple was measured by oscilloscope to be about 1.3 ppm. A trend log

was made for measured variations in the high voltage supply over a period several hours. The maximum total variation measured in any one hour period was 180 mV or 1.8 ppm. The vendor specification is 5 ppm which is predicted to corresponds to a field size variation of 2 nm. It is therefore expected that the maximum high voltage related field size variation is about 0.7 nm/hr.

IIb. DAC Accuracy

Grating patterns for photonic components such as lasers and filters require that the average grating period be precise and that the period variations be negligibly small to produce gratings comparable to those made by laser holographic methods. Even within a single writing field, artifacts can occur if the there exist DAC linearity errors which are systematically embedded in the e-beam written patterns. In order to evaluate the departure from the ideal, we sampled the linearity of the deflection amplifier output errors that occurred at major bit changes in the four primary deflector (X,Y,X+Y,X-Y) and sub deflector (X,Y) DACs. Due to the large number of bits in the defectors, linearity was spot checked at each of the major bit changes (i.e., 2^1, 2^2, 2^3, etc.).

Absolute departures (integrated errors) over the entire DAC range were found to be below 0.5 LSB, which corresponds to a maximum deflection error of less than 0.5 nm. The maximum relative change between consecutive measurements was about two times smaller.

Another sensitive method of testing for the presence of systematic DAC artifacts is to simply expose a large area grating with a sub-optical period. The grating is then examined in an optical microscope equipped with Nomarski contrast. This inspection typically reveals systematic variations in the exposure which are undetectable by SEM inspection. Such an exposure was performed for a 0.24 μm period grating written over a 500 μm field. SEM images were first taken to verify that well resolved gratings were produced at all portions of the field. The corresponding area was then examined in an optical microscope and proved to be completely featureless. This is a good indication that good calibration has been achieved between the sub- and primary- deflectors and that the DACs do not exhibit an observable superstructure.

IIc. Patterning Performance

Since most patterns to be written exceed the dimensions of a single writing field, stitching accuracy can be very important and even limit the use of a tiling type writing strategy. Discontinuities or significant linewidth variations at writing field boundaries can cause electrical breaks or shorts in electronic devices, or phase shifts in photonic components. While all e-beam lithography systems attempt to minimize such errors, the JBX-9300FS further mitigates these effects via a hardware implementation of field shift writing (FSW). This method writes the pattern data n times at 1/n of the exposure dose, with the scan field center shifted each time. The number of overwrites is entered as parameter in the exposure program (n=1 to 5) and the shifted data is calculated by on board processors and loaded automatically into a data buffer. Typically we found improvement in the overall stitching accuracy for up to three overwrites. The FSW data results reported here are for only two overwrites, which is sufficient to realize most of the performance enhancement.

Pattern writing accuracy on a mask blank is based on a calibration procedure in which the laser interferometer stage controller is used as a precise distance standard. This mode of writing on a flat, low expansion substrate offers the best conditions for evaluating the inherent writing errors. The pattern used in this test comprises an ensemble of cross patterns that are written by the e-beam system and whose positions are measured using a Leica LMS IPRO. In particular, a 6 X 6 array of 500 μm field-sized patterns containing crosses within and across field boundaries were written on a 5 inch fused silica mask plate coated with ZEP 7000 resist. This 3mm X 3mm area is small and placed near the center of the plate such that stage runout errors are not significant. The intrafield and interfield errors therefore reflect deflection nonlinearities, deflector noise, and calibration (magnification and rotation) errors.

The exposure and measurement were performed both with and without field shift writing. The results of this multifield placement test for the mask writing mode are plotted in Figure 7 for the FSW (n=2) case. The overall measurements for the 6 X 6 array of fields (in total 884 cross locations measured) are shown. Absolute errors from the ideal locations are plotted using the pattern center determined from a global fit of all the points. The maximum errors observed in the array without FSW were, +16 nm in X and -19nm in Y, while the maximum errors improved to −12 nm in X and +8 nm in Y with FSW (n=2).

At the boundary of 4 fields any rotation or magnification errors should be greatest which usually lead to the observable stitching errors. To quantify the stitching errors, the relative placements errors were measured for marks located in the field corners (F_1, F_2, F_3, F_4) after subtracting the ideal displacements. This region of the pattern accounts for the missing portions of the IPRO map in Fig. 7. The corner marks were pairwise subtracted (F_1 - F_2 , etc) and an error map plotted. This was performed for both the FSW and no-FSW cases. The maximum errors were found to be +/- 14nm with no FSW and these improved slightly to −10 nm/+13 nm with FSW. The field boundaries were indistinguishable from other groups of marks interior to a single field. All of these results fall well within the vendor specs.

Relative error measurements were also made within individual 500μm fields (central 400 μm measured) on mask plates to obtain information about the intra-field placement accuracy. This type of measure eliminates the absolute location of the field, and therefore focuses on the deflector precision. Six fields were measured, three with FSW and three without FSW. The maximum errors with FSW were -7nm in X and +6nm in Y and for no FSW are -12nm in X and -9nm in Y. This FSW measurements are approaching the noise floor of the IPRO measurement system.

A similar assessment was made of the field stitching errors in "direct writing" mode. In direct writing mode, the magnification and rotation calibrations are obtained from marks placed on the wafer from a previous lithography step rather than using the laser interferometer as a metrology standard. Therefore we expect the field stitching result to include the compound errors from these two operations. In addition, this test is performed on a silicon wafer rather than a fused silica mask plate to better simulate performance under device fabrication conditions. Silicon has has a five times higher expansion coefficient and is less rigid.

The placement measurements on the wafers were performed using an e-beam metrology program, ARRAY, similar to the optical IPRO tool. The marks were transferred to the wafer by dry etching prior to measurement to allow reasonable contrast in backscattered electron mode. Four marks (F_1, F_2, F_3, F_4) located in the field corners were measured and pair-wise subtracted to map the positional deviations among the marks at the intersecting corners of the fields. This represents the distribution of field stitching errors during a direct write-on-wafer operation. In total, 100 difference measurements were made (all for the FSW, n=2 case). A representative set (F_1-F_4) of results (25 of the 100) is shown in Figure 8. The errors are again measured from the ideal assuming a center location from global marks. While the errors are small and within the specification, we do observe a systematic increase in the X-gain error to the right. This is likely caused by a slight miscalibration between the deflector gain adjustment and the corresponding height measurement value. The maximum errors for the complete set of four such maps were found to be –21nm in X and +24nm in Y in a 6 X 6 field array (500 μm each).

For device fabrication the level to level alignment is important for tolerancing self-aligned features (eg. transistor gates) with critical dimensions. To test this, two levels were written both using FSW (n=2) on a silicon substrate and aligned to a set of etched fiducial marks previously patterned on the wafer. The alignment marks consist of four marks which are used to adjust the gain, rotation and field distortion. The focusing is entrusted to the height mapping system. The measurement patterns were interleaving arrays of crosses arranged such that alternating fields had a level one and level two crosses at the field center. Measurements were made of these center crosses using the ARRAY program in a JBX 7000MV mask making tool. The arrays written as separate exposures were measured and subtracted element by element from the ideal and the absolute errors plotted. One of three chips measured is shown in Figure 9. The maximum errors recorded for the complete set were –13nm in X and +12nm in Y. The systematic differences in two exposures are evident in the plot, giving rise to the triangle wave appearance across the rows of the plot.

The long range absolute pattern placement accuracy is affected by several factors, some of which are discussed above. It is the sum total of errors in calibration, beam drift, stage positioning, and thermally induced dimension changes during exposure. Accurate assessment can also be difficult since measurements are made using instruments with precision comparable to that of the writing instrument. Overall magnification errors can accumulate over large stage distances (run out) and greater height variations are encountered over larger portions of substrates, therefore placement accuracy typically degrades with increased measurement area. The vendor therefore specifies the placement accuracy as determined by the Leica IPRO metrology system within a 50 mm square area to be < +/- 30 nm rather than over the entire stage travel. To minimize the thermal expansion effects, the (fused silica) mask plate for this test was permitted to equilibrate for several hours (soak time) in the vacuum chamber prior to exposure. A 6 X 6 array of chips on 10 mm centers was written within a 60 mm square centered on the plate. The measured map of the resulting central cross pattern (only the center crosses are used to again separate the placement errors from the deflection errors) is shown in Figure 10. All errors were over this found to be within +/- 16 nm, well within the specification. Since

our planned applications include highly accurate mask making, we performed an additional placement test which spanned a100 mm area on a 5 inch mask plate. The result is shown in Figure 11. The errors approximately scaled linearly, yielding maximum values of –30nm in X and +26nm in Y, still within the vendor spec even over this significantly larger area.

III. SYSTEM ENHANCEMENTS

Since the JBX9300FS is substantially redesigned from previous systems, there are several new features that have been incorporated in addition to the improved hardware described above. The new system includes: a height mapping mechanism which is used to adjust focus on-the-fly, a stepper distortion correction routine which allows proper overlay during mix and match ebeam /optical lithography, a robotic stocker has been added which allows random access to stored cassettes prior to introduction into the vacuum chamber, and a new window based user interface running on a Unix-based personal workstation.

The height mapping system is based on an optical reflection from the substrate and is a two directional system to cancel the effect of substrate tilt. It is intended for use with both masks and patterned wafers. The relevant performance criteria is the reproducibility of the height determination compared with the depth of focus of the electron optical system. A series of height measurements were made for the two directions of the height mapping system. The uncertainty was found to be about 0.1 μm for each direction. This appears to be well within the expected depth of focus for the instrument during normal use.

The mark detection method has also been changed in the new instrument. As the beam is scanned across the alignment mark the backscattered electron detector signal is digitized and accumulated for several scans to achieve some averaging. The derivative is obtained from the resulting waveform. A correlation method [9] is then applied to the derivative signal to exploit the symmetry of the waveform. The derivative is an odd function thereby yielding a sharp negative peak at the mark center location. This method has been shown to improve results under poorer signal to noise conditions.

IV. SOFTWARE

The data format used by the JBX-9300FS (as well as the JBX 9000MV mask writer) is JEOL52 Version 3.0 and is not compatible with earlier versions unless conversion software is used. The new format permits a compaction mode that is directly interpreted by the system hardware. The software supplied with the instrument will accept and convert to JEOL52 v.3.0 the following data formats: JEOL01, JEOL51, GDS II (Stream Format), PG3000, and PG3600. An OVMS personal workstation is used to process these conversions and is capable of graphically displaying and overlaying the data. Third party conversion software is also an option (eg., CATS [10] and CAPROX [11]).

VI. SUMMARY

The overall performance of the JBX-9300FS represents a significant advance over prior generation systems. The principle components appear to be performing at their design levels. The electron optical column, field emission gun, and high voltage supply

combined to produced a stable, sub-7 nm spot over a wide range of beam currents. The large deflection field has made necessary a new dynamic correction scheme to simultaneously keep a finely focused spot while deflecting over larger scan angles. This system appears to work well with settings that remain stable over long periods of use. The stage precision, temperature control and minimal beam drift combined to produced over a factor of three improvement in pattern placement accuracy over the previous generation system.

ACKNOWLEDGEMENTS

We wish to thank H. Noma, H. Yamamoto, and M. Yoshimoto of JEOL Ltd. for their expert technical work in performing many of the test procedures reported here.

REFERENCES

[1] R.E. Howard, H.G. Craighead, L.D. Jackel, and P.M. Mankiewich, M. Feldman, "Electron Beam Lithography from 20 to 120 keV with a High Quality Beam", J. Vac. Sci. Technol. B 1 (4), 1101 (1983).

[2] D. F. Kyser, "Spatial Resolution Limits in Electron Beam Nanolithography", J. Vac. Sci. Technol. B 1 (4), 1391 (1983).

[3] S. Thoms, S.P. Beaumont, and C.D.W. Wilkinson, "A JEOL 100 CXII Converted for Use as an Electron-Beam Lithography System, J. Vac. Sci. Technol. B 7 (6), 1823 (1989).

[4] G.A.C. Jones, S. Blythe, and H. Ahmed, ", J. Vac. Sci. Technol. B 5 (1), 120 (1987).

[5] M.A. McCord, R. Viswanathan, F.J. Hohn, A.D. Wilson, R. Naumann, and T.H. Newman, "100kV thermal field emission electron Beam Lithography Tool for High-Resolution X-ray Mask Pattterning", J. Vac. Sci. Technol. B 10 (6), 2764 (1992).

[6] Leica Microsystems Lithography Ltd., Cambridge, UK

[7] Eiko Engineering Company Ltd., Ibaraki, Japan

[8] H. Takemura, H. Ohki, H. Nakazawa, Y. Nakagawa, M. Isobe, Y. Ochiai, T. Ogura, T. Mogami, M. Narihiro, "Performance of New E-Beam Lithography System JBX-9300FS", Proceedings of Intl. Conference of Micro-and-Nano-Engineering 99,

[9] I. Kawamura et al.: "The Application of the Correlation Method for the EB (Electron Beam) Exposure System" Proc. of 1990 Intern. Microprocess Conference, pp.64-67.

[10] CATS is a trademark of TEL, Transcription Enterprises Ltd., Los Gatos, CA.

[11] CAPROX is a trademark of Sigma-C GmbH, Munich, Germany.

Table 1: JBX 9300 FS Electron Beam Lithography System Performance Results					
Item	Acc Voltage	Conditions	Measurements	Specification	Results
Minimum Beam Size	100 kV	100 pA	Oscilloscope trace of knife edge scan	4+/- 1 nm	X=4.0 nm Y=3.8 nm
Linewidth Uniformity	100 kV	500 μm field ZEP 520	0.1 μm line @ 9 locations	< 30% p-p	Xmin = 100 nm; Xmax = 106 nm Ymin = 104 nm; Ymax = 110 nm
Position Accuracy within Field	100 kV	1.5 nA 500μm field ZEP 7000	Leica IPRO	with FSW: <+/- 0.02μm without FSW: <+/-0.03 μm	with FSW: -0.007μm, +0.006μm w/out FSW: -0.012 μm,+0.009μm
Mask Write: Field Stitching Accuracy	100 kV	1.5 nA 500μm field ZEP 7000	Leica IPRO	with FSW: <+/- 0.02μm without FSW: <+/-0.03 μm	with FSW: -0.010μm, +0.013μm w/out FSW: -0.014 μm,+0.014μm
Direct Write: Field Stitching Accuracy	100 kV	1.5 nA 500μm field ZEP 520	JEOL ARRAY Program	with FSW: <+/-0.03 μm	with FSW: -0.021μm, +0.024μm
Overlay Alignment Accuracy	100 kV	1.5 nA 500μm field ZEP 520	JEOL ARRAY Program	with FSW: <+/-0.03 μm	with FSW: -0.013μm, +0.012μm
Placement Accuracy: 50 mm Mask Area	100 kV	1.5 nA 500μm field ZEP 7000	Leica IPRO	with FSW: <+/-0.03 μm	with FSW: -0.011μm, +0.016μm
Placement Accuracy: 100 mm Mask Area	100 kV	1.5 nA 500μm field ZEP 7000	Leica IPRO	no spec	with FSW: -0.030μm, +0.026μm

FIGURE CAPTIONS

Figure 1. Plot of spot size dependence in X and Y on beam current measured using the knife edge scan data as shown in Fig. 1 for two different apertures.

Figure 2. Beam current densities calculated from the mean values of the X and Y beam diameter measurements plotted in Fig. 2.

Figure 3. SEM images of 0.1μm lines exposed and developed in ZEP 520 resist at the center, edges and corners of the maximum field (500μm) to test the suitability of CD control for wide gate transistor work. CD uniformity is within 3% of the mean linewidth.

Figure 4. SEMs of line and space pattern with a 50 nm pitch exposed at the perimeter and center of a 400μm writing field. Writing parameters are shown in the inset. This test was used to verify that the dynamic focus and stigmation method is suitable for nanolithographic applications over large field areas.

Figure 5. SEM of a line and space pattern in ZEP 520 resist a) at low magnification and b) at high magnification showing 18nm lines on 53 nm centers.

Figure 6. Measured beam drift in position over a 14 hour period. X and Y are plotted separately and each is measured on an upper and lower fiducial mark. The beam remained within 60 nm in X and 25 nm in Y during the measured period, well below the specified limit of 150 nm/hr.

Figure 7. LMS IPRO measurement maps of mask write interfield placement errors with FSW (n=2). Errors are absolute errors from the pattern center. The substrate was a 125 mm fused silica mask blank coated with ZEP 7000 resist.

Figure 8. The e-beam metrology program ARRAY was used to measure and map the direct write interfield stitching errors (with FSW, n=2). This pattern was written on a 150 mm silicon wafer with pattern transfer of the mark pattern by dry etching.

Figure 9. The e-beam metrology program ARRAY was used to produce these results of the overlay test. The error map is obtained from the element by element subtraction of the mark locations exposed during separate writing sessions. This test was performed on a 150 mm silicon wafer.

Figure 10. LMS IPRO measured map of the long range pattern placement accuracy made for an 7 X 7 mark array over a 60 mm X 60 mm area corresponding to the vendor specification. This test performed on a 125 mm fused silica mask plate.

Figure 11. LMS IPRO measured map of the long range pattern placement accuracy made for an 11 X 11 mark array over a 100 mm X 100 mm area, beyond the vendor specified area. This test was performed on a 125 mm fused silica mask plate.

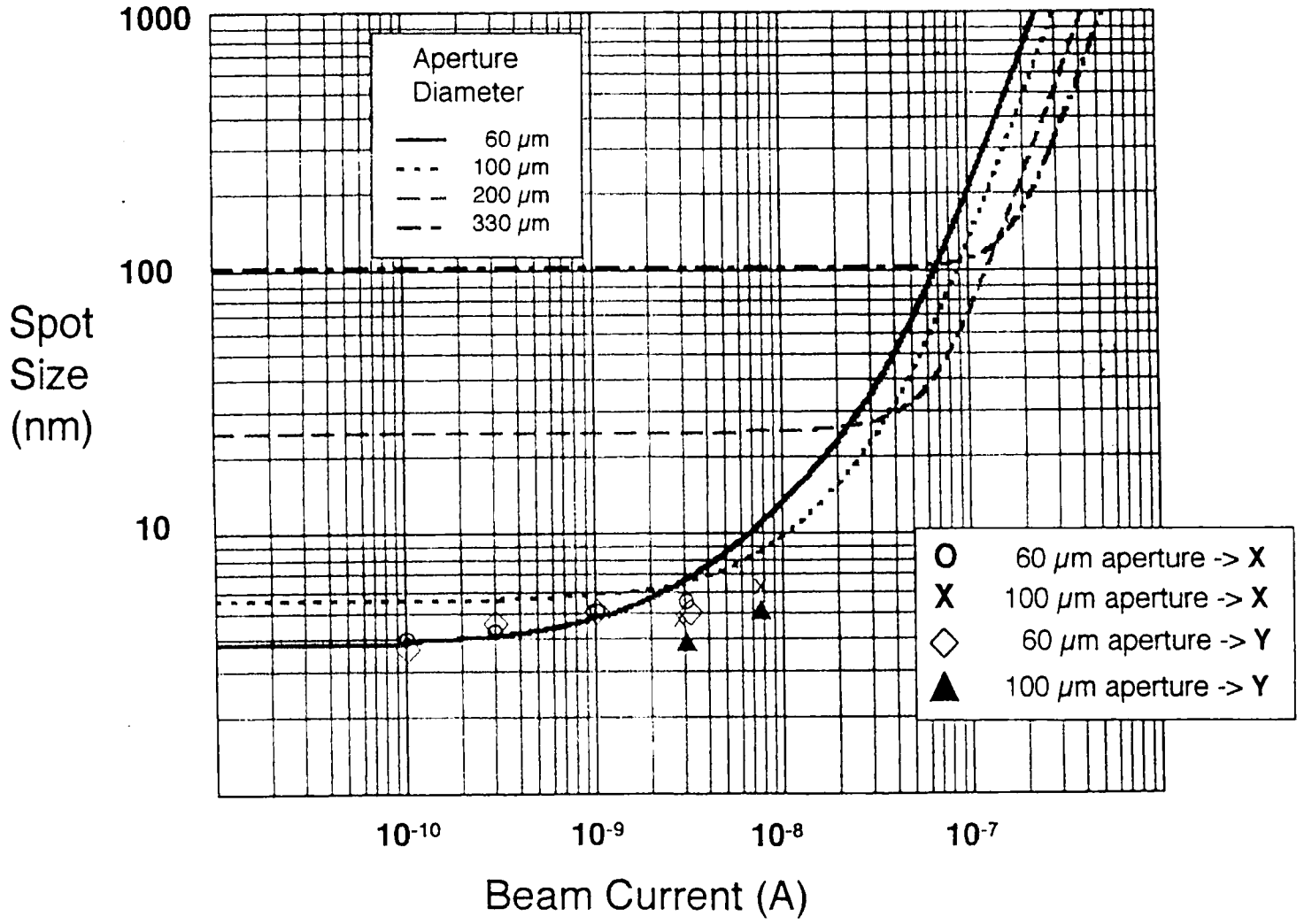
1000
100
10
Spot Size (nm)
Aperture Diameter
60 μm
100 μm
200 μm
330 μm
O 60 μm aperture -> X
X 100 μm aperture -> X
◇ 60 μm aperture -> Y
▲ 100 μm aperture -> Y
10-10
10-9
10-8
10-7
Beam Current (A)

Figure 1

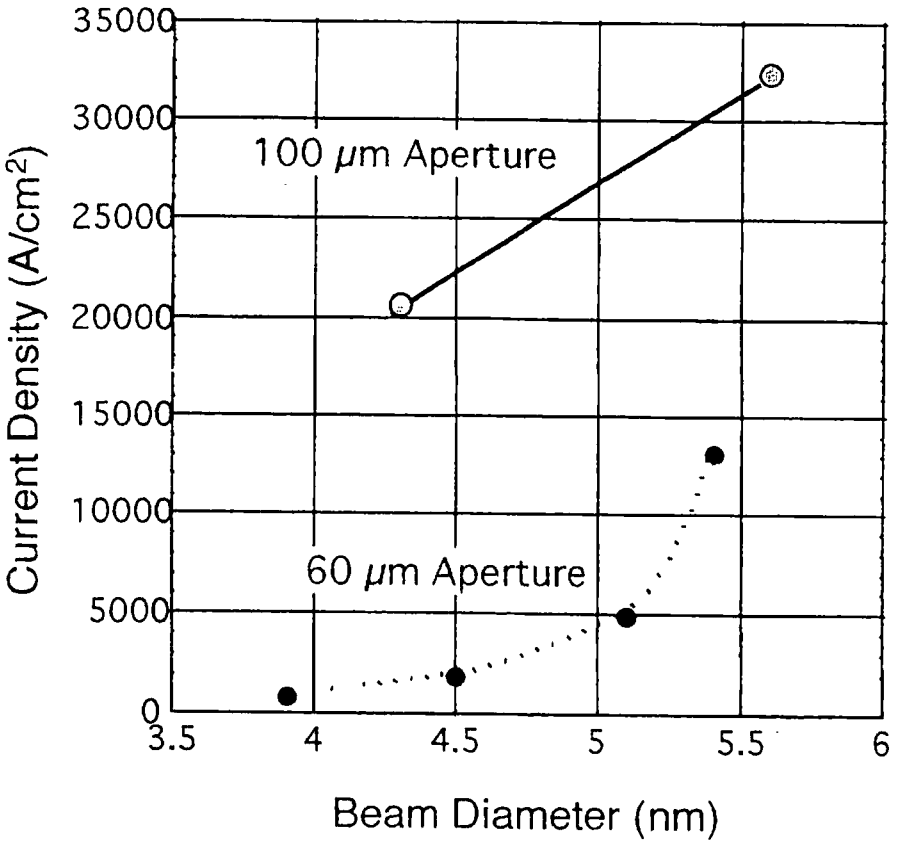
35000
30000
25000
20000
15000
10000
5000
0
Current Density (A/cm²)
100 μm Aperture
60 μm Aperture
3.5
4
4.5
5
5.5
6
Beam Diameter (nm)

Figure 2

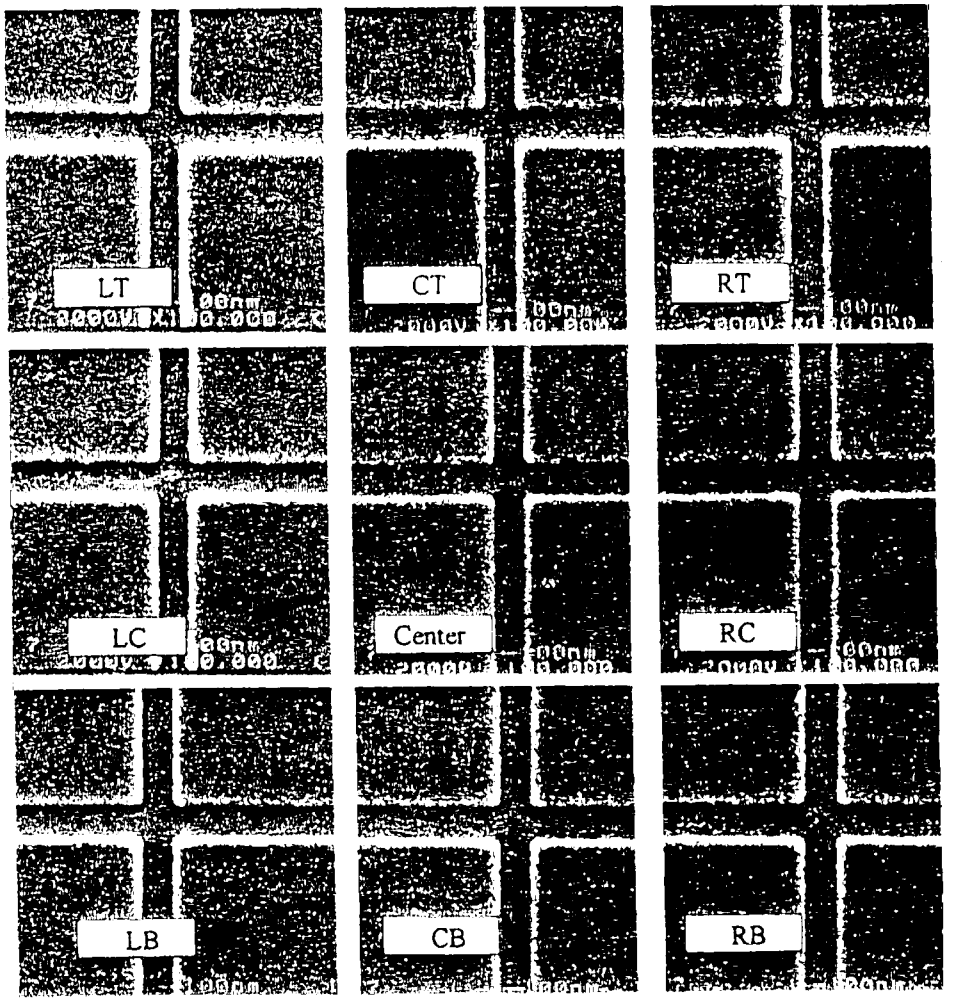

Figure 3

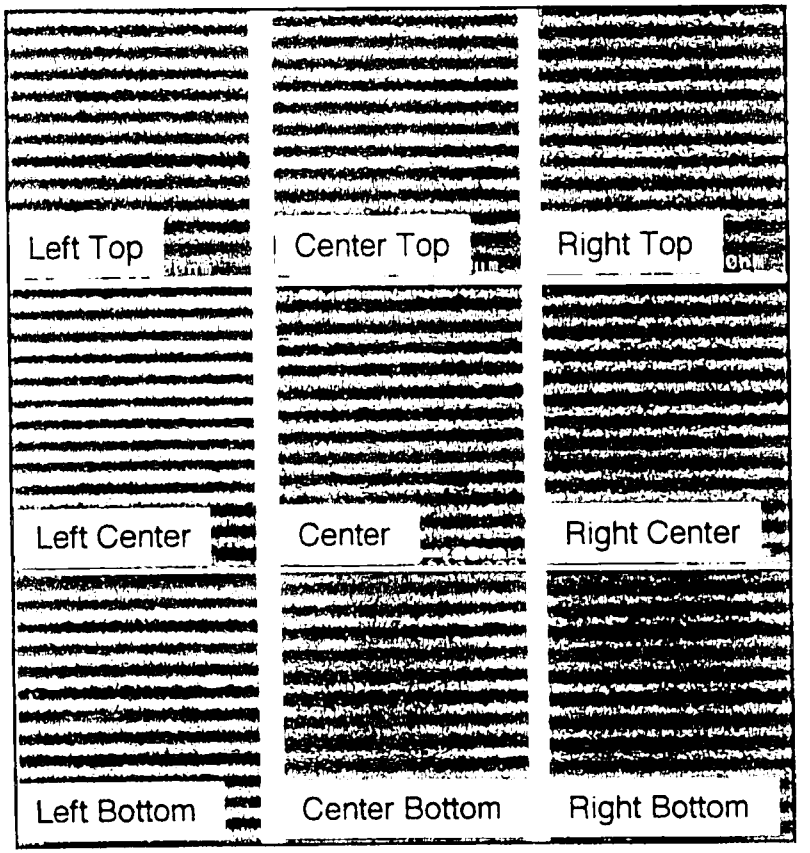
Left Top
Center Top
Right Top
Left Center
Center
Right Center
Left Bottom
Center Bottom
Right Bottom

Figure 4

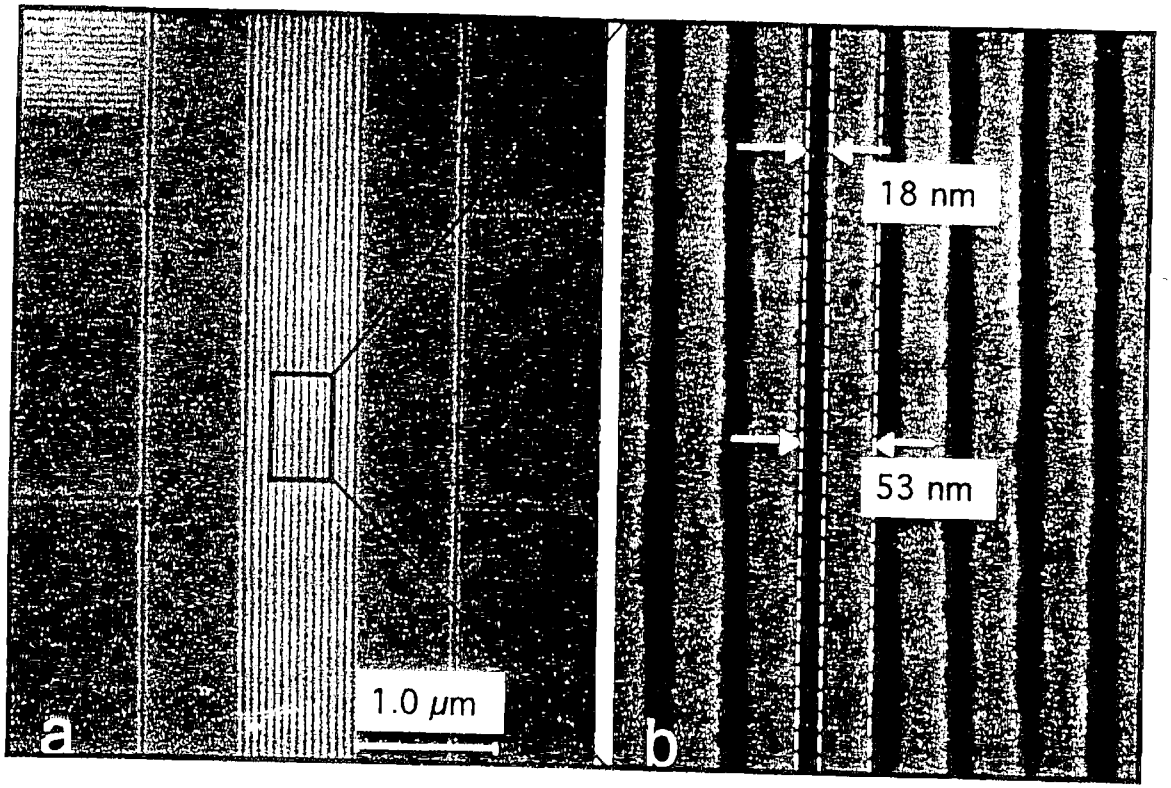

Figure 5

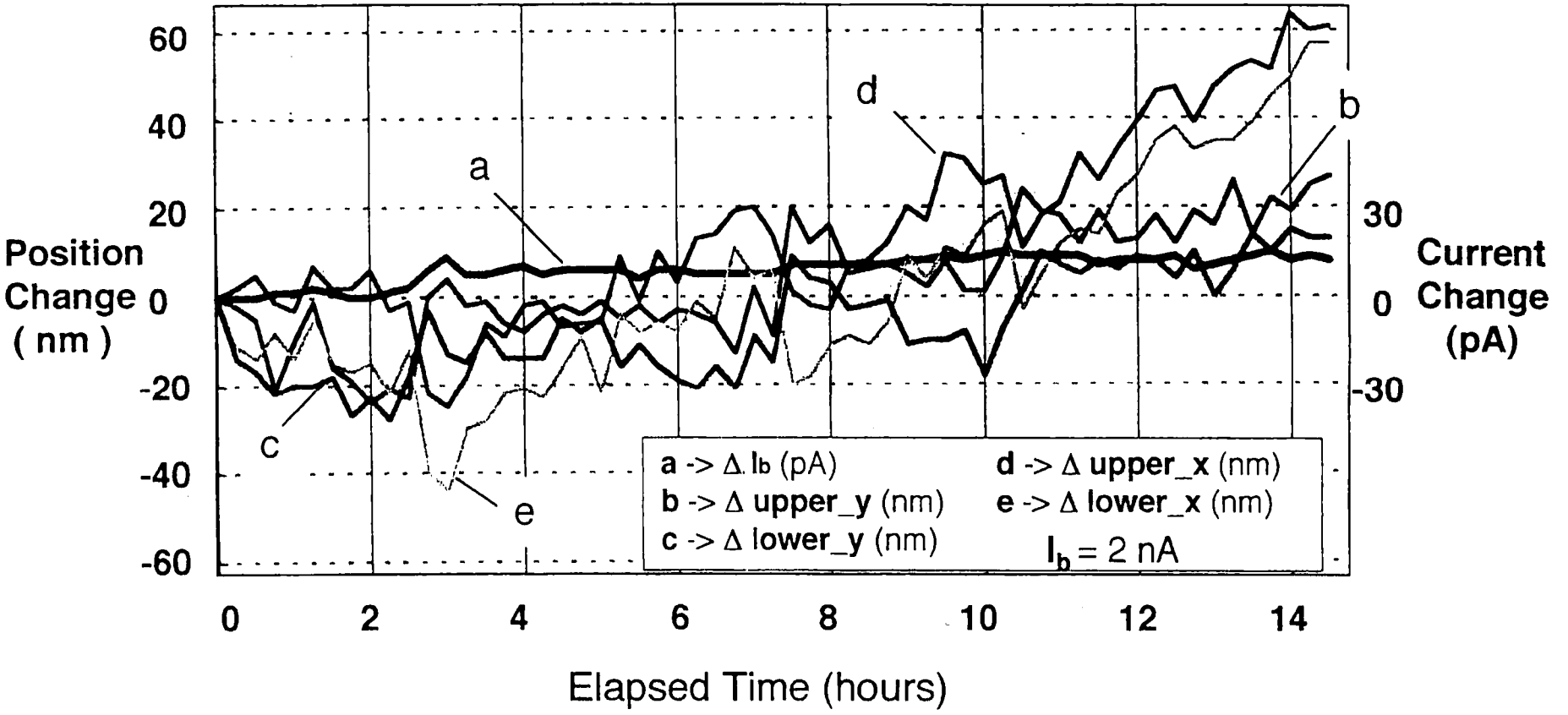
60
40
20
0
-20
-40
-60
Position Change (nm)
30
0
-30
Current Change (pA)
0
2
4
6
8
10
12
14
Elapsed Time (hours)
a
b
c
d
e
a -> Δ Ib (pA)
b -> Δ upper_y (nm)
c -> Δ lower_y (nm)
d -> Δ upper_x (nm)
e -> Δ lower_x (nm)
Ib = 2 nA

Figure 6

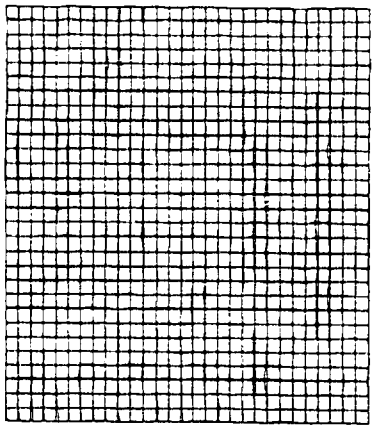

L 0.05 μm

FSW (n=2)

	x(μm)	y(μm)
Mean	0.000	0.000
Max 3σ	0.010	0.009
Min Error	-0.012	-0.008
Max Error	0.011	0.008

Figure 7

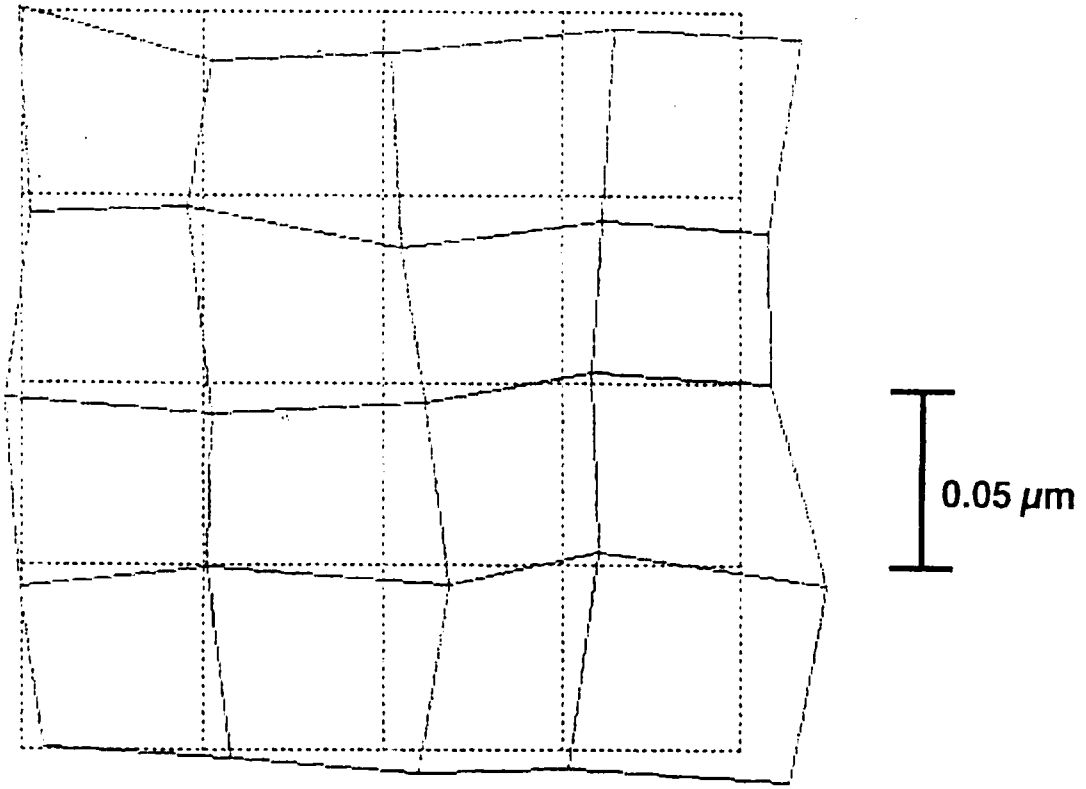

Figure 8

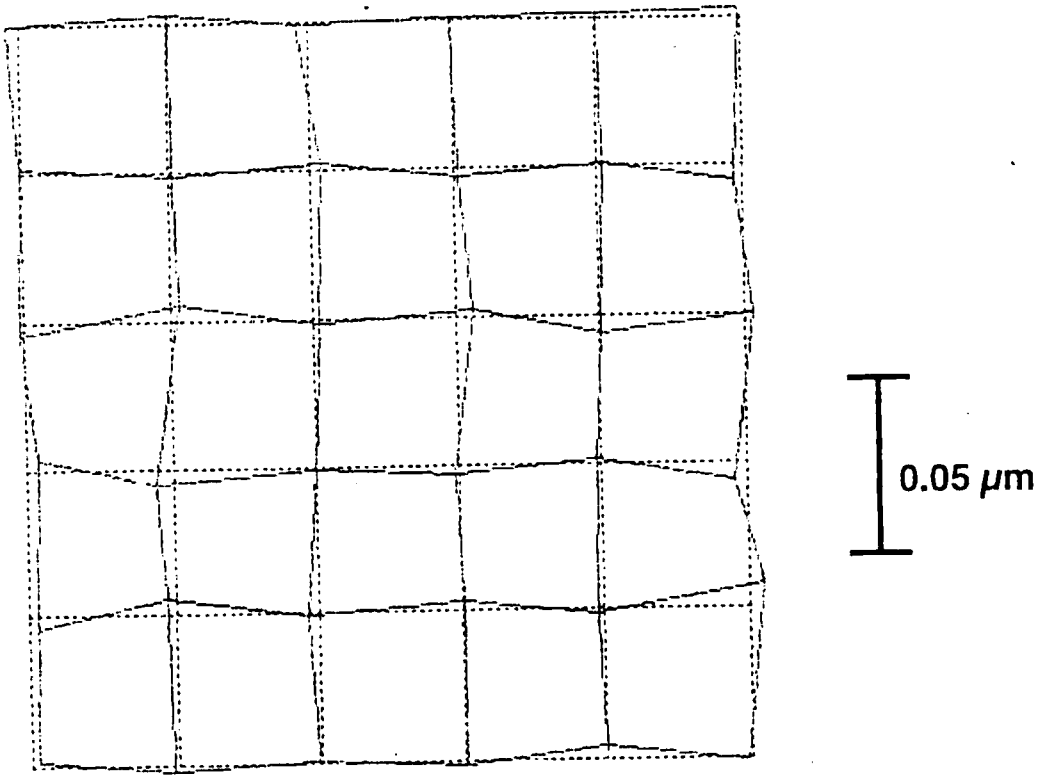

overlay test

Figure 9

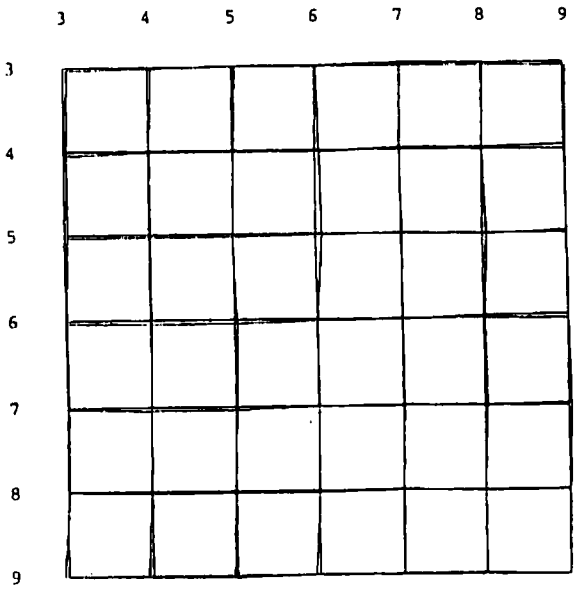

60 X 60 mm

0.05 μm

	x(μm)	y(μm)
Mean	0.003	-0.001
Max 3σ	0.016	0.017
Min Error	-0.011	-0.011
Max Error	0.016	0.011

Figure 10

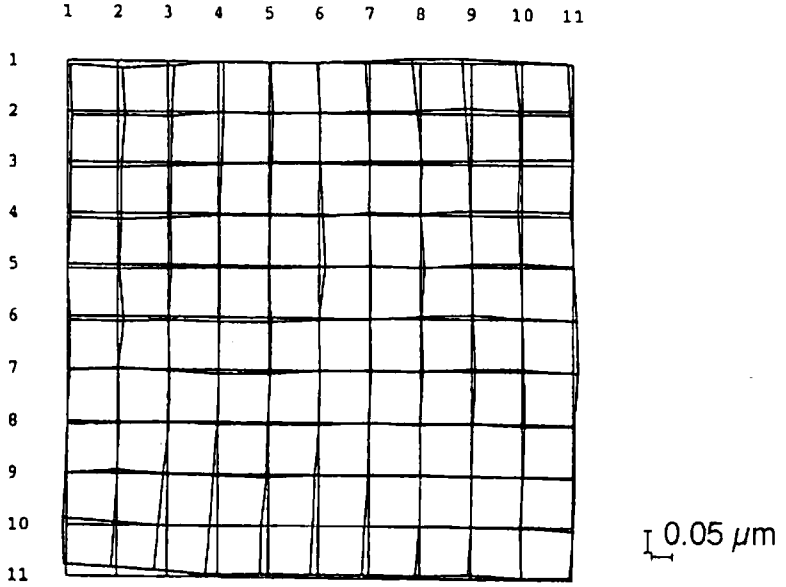

100 X 100 mm	x(μm)	y(μm)
Mean	0.000	0.000
Max 3σ	0.028	0.023
Min Error	-0.030	-0.016
Max Error	0.018	0.026

Figure 11